Atmos. Chem. Phys. Discuss., 15, 8771–8799, 2015
www.atmos-chem-phys-discuss.net/15/8771/2015/
doi:10.5194/acpd-15-8771-2015

Atmospheric Chemistry and Physics Discussions

Effect of gravity wave temperature fluctuations on homogeneous ice nucleation in the tropical tropopause layer

T. Dinh[1], A. Podglajen[2], A. Hertzog[2], B. Legras[3], and R. Plougonven[2]

[1]Program in Atmospheric and Oceanic Sciences, Princeton University, Princeton, New Jersey, USA
[2]Laboratoire de Météorologie Dynamique, École Polytechnique, Palaiseau, France
[3]Laboratoire de Météorologie Dynamique, École Normale Supérieure, Paris, France

Received: 3 March 2015 – Accepted: 8 March 2015 – Published: 24 March 2015

Correspondence to: T. Dinh (tdinh@princeton.edu)

Published by Copernicus Publications on behalf of the European Geosciences Union.

Abstract

The impact of high-frequency fluctuations of temperature on homogeneous nucleation of ice crystals in the vicinity of the tropical tropopause is investigated using a bin microphysics scheme for air parcels. The imposed temperature fluctuations come from measurements during isopycnic balloon flights near the tropical tropopause. The balloons collected data at high frequency, guaranteeing that gravity wave signals are well resolved.

With the observed temperature time series, the numerical simulations with homogeneous freezing show a full range of ice number concentration (INC) as previously observed in the tropical upper troposphere. In particular, low INC may be obtained if the gravity wave perturbations produce a non-persistent cooling rate (even with large magnitude) such that the absolute change in temperature remains small during nucleation. This result is explained analytically by a dependence of the INC on the absolute drop in temperature (and not on the cooling rate). This work suggests that homogeneous ice nucleation is *not* necessarily inconsistent with observations of low INC.

1 Introduction

Cirrus clouds have an important impact on the global radiative energy budget (Lohmann and Roeckner, 1995). In the tropical tropopause layer (TTL, Fueglistaler et al., 2009), cirrus clouds contribute to the radiative heating (Corti et al., 2006; Dinh and Fueglistaler, 2014a) and control the dehydration of the air before entry into the stratosphere (Brewer, 1949; Jensen et al., 1996; Dinh and Fueglistaler, 2014b). For all cirrus clouds, the radiative and climate impact, ability to modify water vapour, and cloud evolution are sensitive to the ice number concentration (e.g. Kärcher et al., 2014), which depends strongly on the nucleation process of ice crystals.

When evaluating the ice number concentration (INC) produced by nucleation, it has been often assumed that the relevant time scale is sufficiently short such that the verti-

ACPD
15, 8771–8799, 2015

cal velocity and associated adiabatic cooling rate remain constant (e.g. Barahona and Nenes, 2008). For constant cooling rate, homogeneous freezing of aqueous aerosols produces higher INC ($> 1000\,L^{-1}$) than those commonly observed ($< 100\,L^{-1}$) in cirrus clouds (Lawson et al., 2008; Krämer et al., 2009; Davis et al., 2010). Observations and calculations of INC based on homogeneous freezing can be reconciled only if very low vertical speeds ($w < 0.01\,m\,s^{-1}$) are used in the simulations. This seems at odds with the ubiquitous presence of atmospheric gravity waves, which typically generate an order of magnitude larger disturbances in the vertical velocity. Therefore, it has been suggested that heterogeneous freezing (instead of homogeneous freezing) is the dominant nucleation mechanism for cirrus clouds in the upper troposphere (Jensen et al., 2010, 2012). The INC obtained by heterogeneous freezing is apparently limited by the availability of suitable ice nuclei (generally less than $100\,L^{-1}$) in the upper troposphere (Chen et al., 1998; Rogers et al., 1998).

However, Spichtinger and Krämer (2013) pointed out that high-frequency variations in temperature and cooling rates can substantially decrease the INC produced during homogeneous nucleation compared to those obtained with constant updraft speeds. Yet, their numerical results are based on ideally constructed temperature time series, and so remain somewhat conceptual. The present work complements their study by using temperature time series data collected at high temporal resolution during long-duration balloon flights near the tropical tropopause. The observed temperatures contain perturbations from a spectrum of atmospheric waves, with periods ranging from days to minutes. Our analysis of the nucleation simulations based on these observed time series confirms the earlier results of Spichtinger and Krämer (2013), and furthermore reveals an exponential relationship between the INC and the absolute change in temperature during the nucleation events.

The article is organised as follows. Sections 2 and 3 describe the balloon data and the technical details of the model used here to simulate homogeneous ice nucleation. Section 4 presents the numerical results. Section 5 provides the theoretical basis ex-

ACPD
15, 8771–8799, 2015

plaining how the fluctuations in time of temperature may affect homogeneous ice nucleation. Section 6 contains the conclusions.

2 Balloon data descriptions

The temperature time series used in this study are derived from data collected by two long-duration, superpressure balloons launched by the French Space Agency from Seychelles Islands (55.5° E, 4.6° N) in February 2010 in the framework of the Pre-Concordiasi campaign (Rabier et al., 2010). The balloons flew at an altitude of about 19 km, and achieved circumterrestrial flights, therefore sampling the whole equatorial area. Details on the balloon trajectories and large-scale atmospheric dynamics during the flights can be found in Podglajen et al. (2014). Superpressure balloons are advected by the wind on isopycnic (constant-density) surfaces and therefore behave as quasi-Lagrangian tracers of atmospheric motions. A further remarkable property of superpressure balloons is their sensitivity to atmospheric gravity waves (Massman, 1978; Nastrom, 1980; Boccara et al., 2008; Vincent and Hertzog, 2014). The sampling frequency of the balloon position, atmospheric pressure and temperature during the campaign is every 30 s.

Here, we do not use the temperature observations gathered during the flights to constrain the nucleation simulations; these time series tend to be both too noisy and warm biased during daytime. Instead, we infer the temperature disturbances from the balloon vertical displacements (ζ'_b), which are obtained by band-pass filtering the raw GPS altitudes to exclude planetary-wave motions (low cut-off frequency $f_{low} = (24\,h)^{-1}$) and balloon own motions (high cut-off frequency $f_{high} = (10\,min)^{-1}$). The high cut-off frequency is sufficiently large to enable us to resolve almost the full spectrum of gravity waves, which extends up to the Brunt–Väisälä frequency ($\sim (4\,min)^{-1}$ in the equatorial lower stratosphere and $\sim (10\,min)^{-1}$ in the TTL). The isentropic air parcel vertical

ACPD
15, 8771–8799, 2015

displacement (ζ') is linked to that of the isopycnic balloon through

$$\zeta' = \frac{g/c_p + \partial\overline{T}/\partial z}{g/R + \partial\overline{T}/\partial z}\zeta'_{\mathrm{b}} \tag{1}$$

(Boccara et al., 2008), where g is the gravitational acceleration, c_p is the specific heat at constant pressure, R_{a} is the gas constant for air, and $\partial\overline{T}/\partial z$ is the vertical gradient of the background temperature. We use the European Centre for Medium-Range Weather Forecasts (ECMWF) operational analyses to diagnose $\partial\overline{T}/\partial z$ at the balloon position in the above equation. The vertical displacement of the air parcel is then converted to the Lagrangian temperature fluctuation at the balloon flight level (i.e. in the lower stratosphere) by

$$T'_{\mathrm{LS}} = -\frac{g}{c_p}\zeta'. \tag{2}$$

We must furthermore take into account that the balloons flew in the lower stratosphere rather than in the upper troposphere where most of the cirrus form. Because of the difference in stability of these two regions, the vertical displacements and hence temperature fluctuations induced by gravity waves are larger in the upper troposphere than in the lower stratosphere. For conservative wave propagation, it can be shown that:

$$T'_{\mathrm{UT}} = \sqrt{\frac{N_{\mathrm{LS}}}{N_{\mathrm{UT}}}}\exp\left(-\frac{\Delta z}{2H}\right)T'_{\mathrm{LS}}, \tag{3}$$

where N_{LS} and N_{UT} respectively are the buoyancy frequencies in the lower stratosphere and upper troposphere, Δz is the difference between the balloon flight and cloud altitudes, H is the atmospheric scale height, and T'_{UT} is the temperature disturbance in the upper troposphere induced by the gravity wave packet observed at the balloon altitude. Typically, $N_{\mathrm{LS}} \sim 2N_{\mathrm{UT}}$, and $T'_{\mathrm{UT}} \sim T'_{\mathrm{LS}}$ if the cirrus forms 4 km below the balloon flight level.

ACPD
15, 8771–8799, 2015

3 Model configurations

We compute homogeneous freezing of aqueous aerosols following Koop et al. (2000), and depositional growth of ice crystals (see e.g. Pruppacher and Klett, 1978) using the bin scheme designed by Dinh and Durran (2012). Ice crystals and aerosol particles that form ice crystals are assumed to be spherical.

The time step used in the simulations is 0.5 s. We use 25 bins to resolve the size distribution of ice crystals with radii up to 25 µm. The numerical results do not change for smaller time step and more bins, i.e. the stated time and bin resolutions are sufficient to ensure accuracy.

The number concentration of the aerosol reservoir is $N_a = 200\,\mathrm{cm}^{-3}$, and aerosol particles are assumed to be monodispersed in size with a radius of 0.25 µm. These assumptions are within observed properties of aerosols in the upper troposphere (Chen et al., 1998). Simulations with polydispersed aerosols up to 1 µm in size do not show qualitative differences, and so we retain a monodispersed distribution to simplify the analytical derivation in Sect. 5.

We do not consider ice sedimentation in order to focus solely on the nucleation process. However, if ice sedimentation were included in the simulations, the INC would be reduced. This would further strengthen our point that the INC in cirrus clouds formed by homogeneous freezing could be small.

Currently, the microphysics of ice at the molecular levels is still not well understood. As a consequence, there is not a well constrained limit on the deposition coefficient (also called accommodation coefficient). The deposition coefficient controls the number of gas molecules that effectively enter the condensed phase after a collision with the ice surface. Laboratory measurements of the deposition coefficient vary by as much as three orders of magnitude, between 0.001 and 1 (Magee et al., 2006; Skrotzki et al., 2013). Here we present simulations with $\alpha = 0.001$, 0.05, and 1.

ACPD
15, 8771–8799, 2015

4 Numerical simulations

For adiabatic motions, the effect of pressure variations on the water vapour mixing ratio (r) can be neglected compared with that due to temperature variations. Assuming constant air pressure, we prescribe an initial water vapour content for the air parcels such that nucleation occurs at a chosen temperature T_0. This is possible because the saturation ratio at the threshold of nucleation S_{nuc} is a function of temperature (Koop et al., 2000; Kärcher and Lohmann, 2002; Ren and Mackenzie, 2005), and it is related to the initial water vapour mixing ratio of air parcels by

$$r_0 = \frac{e_{\mathrm{sat}}(T_0) S_{\mathrm{nuc}}(T_0)}{p} \frac{R_{\mathrm{a}}}{R_{\mathrm{v}}}, \tag{4}$$

where e_{sat} is the saturation water vapour pressure, and R_{a} and R_{v} are respectively the gas constants of air and water vapour. The notations $e_{\mathrm{sat}}(T_0)$ and $S_{\mathrm{nuc}}(T_0) \equiv S_0$ refer to respectively e_{sat} and S_{nuc} at T_0. Note that, up to the nucleation time the vapour mixing ratio r is conserved. As illustrated in Fig. 1, every air parcel follows an isoline of constant water vapour mixing ratio ($r = r_0$) until crossing the $S_{\mathrm{nuc}}(T)$ curve, at which point nucleation begins.

The simulations were first carried out for pressure $p = 100\,\mathrm{hPa}$, nucleation temperature $T_0 = 195\,\mathrm{K}$, and deposition coefficient $\alpha = 0.05$ (Sects. 4.1, 4.2, and 4.3.1). A nucleation event is defined to start when the rate of nucleation exceeds a threshold J_ε, and to end when it becomes less than J_ε. For our simulations, choosing a threshold of $J_\varepsilon = 1\,\mathrm{L}^{-1}\,\mathrm{s}^{-1}$, we have $S_0 = 1.509$ for $T_0 = 195\,\mathrm{K}$. Sensitivities to T_0 in the range between 180 and 210 K, and α in the range between 0.001 and 1 are discussed in Sects. 4.3.2 and 4.3.3. Time series of temperature is defined by

$$T(t) = T_0 + T'(t), \tag{5}$$

where $T'(t)$ are either idealised following temperature variations associated with constant and time-varying vertical velocities (Sects. 4.1 and 4.2), or taken from the balloon data (Sect. 4.3).

ACPD
15, 8771–8799, 2015

4.1 Constant vertical velocity

Here temperature is set to decrease with time due to adiabatic cooling at a constant vertical velocity in a hydrostatic background, i.e.

$$T'(t) = -\frac{g}{c_p} w t. \tag{6}$$

We simulated five nucleation events with $w = 10^k\,\mathrm{m\,s^{-1}}$, where $k = \{-3, \ldots, 1\}$.

As shown in Fig. 2 (blue circles), for $w < 1\,\mathrm{m\,s^{-1}}$ the number of ice crystals nucleated N_i increases with w. For $w \geq 1\,\mathrm{m\,s^{-1}}$, all aerosols particles form ice, hence $N_\mathrm{i} = N_\mathrm{a} = 200\,\mathrm{cm^{-3}}$. Figure 2 shows that if the vertical velocity and the cooling rate are constant during the nucleation events, w must be less than $0.01\,\mathrm{m\,s^{-1}}$ in order that $N_\mathrm{i} \leq 100\,\mathrm{L^{-1}}$. This result is consistent with previous studies (e.g. Krämer et al., 2009) of homogeneous freezing under constant vertical velocity.

4.2 Nonpersistent cooling

Here we vary w with time so that the rate of change of temperature $\frac{\mathrm{d}T}{\mathrm{d}t}$ is no longer constant with time. Specifically, we set

$$w(t) = \begin{cases} +0.02\,\mathrm{m\,s^{-1}} & \text{if } t \leq t_\mathrm{s}, \\ -0.02\,\mathrm{m\,s^{-1}} & \text{if } t > t_\mathrm{s}. \end{cases} \tag{7}$$

The time t_s at which w and hence $\frac{\mathrm{d}T}{\mathrm{d}t}$ switch signs is varied by setting $t_\mathrm{s} = \{20; 24; 28; 32; 36\}$ min. Figure 3 shows the evolution of temperature, saturation ratio and INC during the five nucleation events forced by $w = \pm 0.02\,\mathrm{m\,s^{-1}}$ as defined above.

In the two events where w switches signs at 32 and 36 min (blue curves in Fig. 3), the maximum saturation ratio (S_max) is obtained at $t = t^*$ (31 min) before the minimum temperature (T_min) is reached. The saturation ratio decreases after t^* because water

ACPD
15, 8771–8799, 2015

vapour is depleted by depositional growth of ice crystals (even though T continues to decrease). The simulations show that as long as $t_s > t^*$, then the switch at t_s does not significantly affect N_i. The INC in these two events (see Fig. 2, overlapping open blue circles) is almost the same and equal to that which would have been obtained if w were kept constant at 0.02 m s^{-1}. We refer to these events as "vapour-limit," indicating that N_i is limited by the depletion of water vapour in these cases.

For the other three events in which w switches signs before 31 min (red curves in Fig. 3 and open red cirles in Fig. 2), N_i is significantly smaller than for the two vapour-limit events described above. For these three events, S_{max} and T_{min} occur at the same time. After S_{max} is reached, S decreases because temperature increases. We refer to these events as "temperature-limit" because the minimum temperature alone determines S_{max} and hence N_i. The depletion of water vapour by ice depositional growth can be neglected because N_i is small.

The numerical results show that homogeneous ice nucleation may be cut off if the cooling that initiates nucleation does not persist sufficiently long into the nucleation events. As a consequence, low INC can be obtained for temperature-limit events with initially high vertical velocities and cooling rates. The results in this section are consistent with the simulations with similar setups that have been carried out previously by Spichtinger and Krämer (2013).

4.3 Balloon temperature time series

In contrast to the previous sections which used theoretically constructed temperature time series, the numerical simulations presented in this section were carried out using the balloon data. Below, for Sect. 4.3.1 we use T_0 = 195 K and α = 0.05 (same as previously in Sects. 4.1 and 4.2). In Sects. 4.3.2 and 4.3.3, we vary T_0 between 180 and 210 K, and α between 0.001 and 1 to explore sensitivities to these parameters.

ACPD
15, 8771–8799, 2015

4.3.1 Control simulations with T_0 = 195 K and α = 0.05

The evolution of the saturation ratio and temperature during representative nucleation events simulated using the balloon data are shown in Fig. 4. The duration τ of the nucleation events simulated with the observed temperature data ranges from a few minutes up to about an hour. Because of the high-frequency fluctuations in the observed temperature time series, the cooling rate is typically not constant during a nucleation event. Moreover, more than one local maxima and minima in T and S may occur during one nucleation event. Nevertheless, it is possible to distinguish between

- vapour-limit events, for which the absolute maximum S_{max} is obtained before the absolute minimum T_{min} because of substantial vapour depletion; constant cooling rate is a special case of this type, and
- temperature-limit events, for which S_{max} is obtained at the same time as T_{min}; temperature controls the cutoff of nucleation, and vapour depletion is negligible.

Note that the above definitions of the types of events are not based on the duration τ of nucleation. In fact, the time scales of temperature-limit events and those of vapour-limit events are not statistically different (see Fig. 4).

As shown in Fig. 5, the INC nucleated during temperature-limit events is consistently smaller than for vapour-limit events. The numerical results suggest that, for all nucleation events, N_i increases exponentially with the difference

$$\Delta S \equiv S_{max} - S_0 \tag{8}$$

as long as $N_i \ll N_a$ (Fig. 5). For temperature-limit nucleation events, N_i increases exponentially with $|\Delta T|$, where

$$\Delta T \equiv T_{min} - T_0. \tag{9}$$

ACPD
15, 8771–8799, 2015

4.3.2 Sensitivity of INC to nucleation temperature

Here, we prescribe the initial vapour content r_0 of the air parcels such that the nucleation temperature is either $T_0 = 180$ or 210 K. In Fig. 1, this is equivalent to choosing another isoline of r and displacing accordingly the values of T_0 and S_0 at nucleation. As in the previous section, the balloon temperature perturbations are added to these nucleation temperatures to obtain the temperature time series $T(t)$, see Eq. (5).

The number of ice crystals nucleated for $T_0 = 180$ and 210 K is shown in Fig. 6. The data for $T_0 = 195$ K shown previously in Fig. 5 generally lie between the data points for $T_0 = 180$ and 210 K, that is, there is a monotonic relationship between N_i and T_0. For the same ΔS, N_i is smaller for smaller T_0. Conversely, for the same ΔT, N_i is smaller for larger T_0.

4.3.3 Sensitivity of INC to deposition coefficient

The number of ice crystals nucleated at $T_0 = 195$ K for $\alpha = 0.001$ and $\alpha = 1$ is shown in Fig. 7. Notice that the transition from temperature-limit events to vapour-limit events occur at lower INC for $\alpha = 1$ than $\alpha = 0.001$. This makes sense because the ice crystals deplete water vapour at a faster rate in the case $\alpha = 1$, and so the number of ice crystals needed to significantly deplete water vapour is smaller.

For temperature-limit events, the functional dependence of N_i on ΔS (or ΔT) is invariant for different values of α, i.e. N_i is independent of α. However, for vapour-limit events, N_i is smaller for $\alpha = 1$ than $\alpha = 0.001$ for the same ΔS (or ΔT). The sensitivity of vapour-limit events to the deposition coefficient is explained in the theory section below.

5 Theory and discussions

In this section we provide the theoretical basis that explains the numerical results shown previously in Sect. 4.

ACPD
15, 8771–8799, 2015

5.1 Formula for ice number concentration

The rate of nucleation of ice crystals during a nucleation event is given by

$$\frac{dN}{dt} = (N_a - N)JV_a, \tag{10}$$

where N_a is the aerosol particle number concentration, V_a is the volume of each aerosol particle, and J is the homogeneous nucleation rate given by Koop et al. (2000, their Eq. 7). By integrating Eq. (10) from the beginning ($t = t_0$) to end ($t = t_0 + \tau$) of the nucleation event we obtain

$$\ln\left(1 - \frac{N_i}{N_a}\right) = -V_a \int_{t_0}^{t_0+\tau} J dt = -V_a J_{max} \int_{t_0}^{t_0+\tau} \exp(\ln(J) - \ln(J_{max}))dt, \tag{11}$$

where $J_{max} \equiv J(t^*)$ is the maximum value of J during the nucleation event ($t_0 < t^* < t_0 + \tau$), and $N_i \equiv N(t_0 + \tau)$ is the INC obtained at the end of the nucleation event. Following the steepest descent method, we obtain

$$\ln\left(1 - \frac{N_i}{N_a}\right) \approx -V_a J_{max} \int_{t_0}^{t_0+\tau} \exp\left(\frac{1}{2}\frac{d^2(\ln J)}{dt^2}(t^*)(t - t^*)^2\right) dt, \tag{12}$$

$$\ln\left(1 - \frac{N_i}{N_a}\right) \approx -V_a J_{max} \int_{t_0-t^*}^{t_0+\tau-t^*} \exp(-\mu^2 t^2)dt \approx -V_a J_{max} \int_{-\infty}^{\infty} \exp(-\mu^2 t^2)dt, \tag{13}$$

$$\ln\left(1 - \frac{N_i}{N_a}\right) \approx \sqrt{\pi} V_a \frac{J_{max}}{\mu}, \tag{14}$$

where

$$\mu^2 = -\frac{1}{2}\frac{d^2(\ln J)}{dt^2}(t^*) = -\frac{1}{2J_{max}}\frac{d^2 J}{dt^2}(t^*). \tag{15}$$

ACPD
15, 8771–8799, 2015

The approximations used in Eq. (13) is appropriate if $t^* - t_0$ and $t_0 + \tau - t^*$ are both significantly larger than the e-folding time scale given by μ^{-1}. These criteria are well satisfied in our simulations. From Eq. (14) we now have

$$N_i \approx N_a \left(1 - \exp\left(-\sqrt{\pi} V_a \frac{J_{max}}{\mu}\right)\right). \quad (16)$$

For homogeneous ice nucleation, J is given by (see Koop et al., 2000)

$$\log_{10}(J) = P_3(S a_w), \quad (17)$$

where P_3 denotes a third order polynomial, and a_w is the activity of water. Hence

$$\log_{10}(J_{max}) = P_3(S_{max} a_w(T(t^*))) \approx P_3(S_0 a_w(T_0) + \Delta S a_w(T_0)), \quad (18)$$

where ΔS is the change in the saturation ratio during the nucleation event defined in Eq. (8). Since a_w and S_0 are both functions of temperature, J_{max} is a function of ΔS and temperature. Therefore, Eqs. (16) and (18) indicate that N_i is a function of ΔS, μ, and temperature. However, note that ΔS, μ, and temperature are not exclusively independent variables. In fact, substituting Eqs. (17) and (18) into Eq. (15) we obtain

$$\mu^2 \approx f(\Delta S, T_0)\left(\frac{d^2 S}{dt^2}(t^*)\right) + g(\Delta S, T_0)\frac{dS}{dt}(t^*)\frac{dT}{dt}(t^*) + h(\Delta S, T_0)\left(\frac{d^2 T}{dt^2}(t^*)\right), \quad (19)$$

where $f(\Delta S, T_0)$, $g(\Delta S, T_0)$ and $h(\Delta S, T_0)$ are functions of ΔS and T_0, and we have made the approximation that $T \approx T_0$ because the perturbation T' is small compared with T and T_0. Equation (19) indicates that μ is a function of ΔS, temperature, $\frac{dS}{dt}(t^*)$ and $\frac{dT}{dt}(t^*)$.

For the nucleation events at $T_0 = 195\,\mathrm{K}$ shown in Fig. 5, our calculations indicate that $0.01 < \mu < 0.1\,\mathrm{s}^{-1}$. From Eq. (16) we deduce that the large range of N_i (10^{-3} to $10^6\,\mathrm{L}^{-1}$) obtained for these nucleation events must be due to a large range in J_{max}. If the

ACPD
15, 8771–8799, 2015

differences in μ among the nucleation events can be ignored, at a chosen temperature N_i depends solely on J_{max}, which depends solely on ΔS. In fact, setting $\mu = 0.02\,s^{-1}$ and $T_0 = 195\,K$ in Eqs. (16) and (18) we obtain a functional dependence of N_i on ΔS (the solid curve in Fig. 5a) that fits the numerical data well. The error that results from assuming constant μ is further discussed in Sect. 5.2.

For the special case of a temperature-limit event, the partial pressure of water vapor can be approximated as constant during the nucleation event for $t_0 < t < t_0 + \tau$, and so

$$\Delta S \approx -\frac{S_0 L_s}{R_v T_0^2} \Delta T, \tag{20}$$

where ΔT is the change in temperature during the nucleation event defined in Eq. (9), L_s is the latent heat of sublimation, and R_v is the gas constant of water vapour. With $\mu = 0.02\,s^{-1}$ and $T_0 = 195\,K$, from Eqs. (16)–(20) we obtain the solid curve in Fig. 5b that captures the dependence of N_i on ΔT as suggested by the simulations of temperature-limit events.

5.2 Sensitivity of INC to nucleation temperature and deposition coefficient

Using the formulae derived in Sect. 5.1 we can now explain the sensitivity of the numerical results to T_0 and the deposition coefficient α.

In Fig. 6 the two solid curves are obtained for $T_0 = 180\,K$ and $T_0 = 210\,K$ from Eqs. (16)–(20) with $\mu = 0.02\,s^{-1}$. Figure 6a shows that the analytical formulae explain well the pattern of N_i vs. ΔS, except for vapour-limit events at $T_0 = 210\,K$ that produce more than $10^4\,L^{-1}$ ice crystals. This error is associated with the assumption that μ is the same for all ΔS. In fact, Eq. (19) indicates that the partial derivative of μ with respect to ΔS depends on temperature. For higher temperature, calculation of N_i (especially for vapour-limit events) must account for the variations in μ as ΔS varies. As also shown in Fig. 6b, the derived formulae explain well the pattern of N_i vs. ΔT for

ACPD
15, 8771–8799, 2015

temperature-limit events. For vapour-limit events, Eq. (20) overestimates N_i because it neglects the depletion of water vapour during the nucleation events.

For $\alpha = 0.001$ and $\alpha = 1$, the INC obtained for $T_0 = 195\,\mathrm{K}$ is shown in Fig. 7. Equations (16)–(20) predict that the relationship between N_i and ΔS for all events, and the relationship between N_i and ΔT for temperature-limit events do not change with the deposition coefficient. These theoretical predictions are shown by the solid curves in Fig. 7 obtained with constant $\mu = 0.02\,\mathrm{s}^{-1}$. For $\alpha = 1$, the theoretical curve overestimates N_i for vapour-limit events that produce more than $10^3\,\mathrm{L}^{-1}$ ice crystals (Fig. 7a). We attribute this error to the assumption that μ is constant over the shown range of ΔS. In fact, the deposition coefficient governs the growth rate of ice crystals and affects how the saturation ratio changes with time, and how μ changes with ΔS (a consequence of Eq. 19). Our calculations indicate that the partial derivative of μ with respect to ΔS increases with α. For high values of α, calculation of N_i (especially for vapour-limit events) must account for the variations in μ as ΔS varies.

5.3 Dependence of INC on the initial water vapour mixing ratio

The temperature time series $T(t)$ along the trajectory of an air parcel (recall Eq. 5) and the initial water vapour content r_0 of the parcel are two independent conditions to be specified for the simulations. The initial water vapour content r_0 has a one-to-one relationship with the temperature at the threshold of nucleation T_0 via Eq. (4). In Sect. 4 we have studied how the INC varies with the various forms of $T(t)$ for a *given* r_0 and a corresponding T_0. Here, on the other hand, we discuss how the INC varies as r_0 and T_0 vary for a *given* $T(t)$.

Now, consider air parcels with slightly different initial water vapour mixing ratios, r_0 and $r_0 + \delta r_0$. The nucleation temperatures for these air parcels are respectively T_0 and $T_0 + \delta T_0$ (see illustration in Figs. 1 and 8). For constant pressure, δr_0 and δT_0 are related

ACPD
15, 8771–8799, 2015

by

$$\frac{\delta r_0}{r_0} = \frac{\delta e_{\mathrm{sat}}}{e_{\mathrm{sat}}} + \frac{1}{S_0}\frac{\mathrm{d}S_0}{\mathrm{d}T_0}\delta T_0 = \frac{L_{\mathrm{s}}}{R_{\mathrm{v}}T_0^2}\delta T_0 + \frac{1}{S_0}\frac{\mathrm{d}S_0}{\mathrm{d}T_0}\delta T_0 \tag{21}$$

by Eq. (4) and the Clausius–Clapeyron relation. The first term dominates the right hand side of Eq. (21), from which we obtain

$$\frac{\mathrm{d}T_0}{\mathrm{d}r_0} \approx \frac{R_{\mathrm{v}}T_0^2}{L_{\mathrm{s}}r_0}, \tag{22}$$

which indicates that T_0 increases monotonically with r_0. For a given temperature time series $T(t)$, the minimum temperature T_{min} experienced by the parcels is the same (see Fig. 8). It follows that $|\Delta T| = T_0 - T_{\mathrm{min}}$ increases monotonically with r_0. For temperature-limit events, N_{i} increases exponentially with $|\Delta T|$ (recall Fig. 5 and Eq. 20), and so it must increase exponentially with r_0. As r_0 increases, N_{i} increases until reaching a limit above which the nucleation event must be vapour-limit (see e.g. Fig. 5). Thus, for a given temperature time series, r_0 controls N_{i} and also determines whether the nucleation event is temperature- or vapour-limit.

For example, consider a temperature time series defined by a minimum of $T_{\mathrm{min}} = 194.7\,\mathrm{K}$, a cooling rate associated with $w = +0.02\,\mathrm{m\,s^{-1}}$ before T_{min} is reached, and a warming rate associated with $w = -0.02\,\mathrm{m\,s^{-1}}$ after T_{min} is reached (see Fig. 8). This temperature time series is similar to the profiles we have studied earlier in Sect. 4.2. Consider three air parcels following this temperature time series, but for which $r_0 = \{1.77; 1.79; 1.81\} \times 10^{-5}\,\mathrm{kg\,kg^{-1}}$. All three air parcels experience nucleation, and in all cases $T_{\mathrm{min}} = 194.7\,\mathrm{K}$ occurs during the nucleation periods. However, our calculations give $T_0 = \{194.9; 195.0; 195.1\}\,\mathrm{K}$ and $N_{\mathrm{i}} = \{4.8 \times 10^{-1}; 8.4 \times 10^{1}; 3.6 \times 10^{3}\}\,\mathrm{L^{-1}}$ respectively for the three parcels. Moreover, the two drier air parcels experience temperature-limit nucleation events, whereas the moist air parcel experiences a vapour-limit event. As illustrated here, small differences in r_0 result in many orders of magnitude changes

ACPD
15, 8771–8799, 2015

in N_i. Such a strong dependence of N_i on r_0 could explain the large-amplitude, small-scale heterogeneities in the INC as observed in cirrus clouds by Jensen et al. (2013).

6 Conclusions

We have simulated homogeneous ice nucleation using temperature time series data collected at high frequency by long-duration balloon flights near the tropical tropopause. The simulated nucleation events can be conceptually categorised as either vapour-limit or temperature-limit. For vapour-limit events, nucleation is limited by the depletion of water vapour. In contrast, for temperature-limit events, nucleation is controlled by the fluctuations in temperature (while the depletion in water vapour is negligible). The INC obtained for temperature-limit events is smaller than that obtained for vapour-limit events.

Our calculations of temperature-limit events confirm the finding by Spichtinger and Krämer (2013) that high-frequency fluctuations in temperature may limit the INC obtained by homogeneous freezing. Indeed, small INC is obtained if the gravity waves produce large but non-persistent cooling rates such that the absolute drop in temperature (i.e. the difference between the temperature at the threshold of nucleation and the minimum temperature obtained during nucleation) remains small. This relationship between the INC and temperature has been illustrated here both empirically and analytically.

In addition to the fluctuations in temperature, small variations in the initial water vapour content of the air parcels can also lead to large variations in the INC obtained by nucleation. Moreover, post-nucleation processes acting during the cirrus life cycle contribute to modify the cloud original characteristics. Simulations of cirrus clouds in the TTL by Dinh et al. (2012, 2014) show that the INC decreases by several orders of magnitude as the cloud ages. For these reasons, we suggest that homogeneous ice nucleation (even acting alone in the absence of heterogeneous freezing) is not incon-

ACPD
15, 8771–8799, 2015

sistent with recent observations of cirrus clouds in the TTL, that indicate generally low but highly variable INC (Jensen et al., 2013).

Finally, it is encouraging that the INC for temperature-limit events does not depend on the deposition coefficient, a parameter still poorly constrained by theoretical understanding as well as laboratory measurements and field observations.

Acknowledgements. The data used for simulations in this work was collected during the project "Concordiasi," which is supported by the following agencies: Météo-France, CNES, CNRS/INSU, NSF, NCAR, University of Wyoming, Purdue University, University of Colorado, Alfred Wegener Institute, Met Office, and ECMWF. Concordiasi also benefited from the logistic and financial support of the Institut polaire français Paul Emile Victor (IPEV), Programma Nazionale di Ricerche in Antartide (PNRA), United States Antarctic Program (USAP), British Antarctic Survey (BAS), and from measurements by the Baseline Surface Radiation Network (BSRN) at Concordia.

Tra Dinh acknowledges support from the NOAA Climate and Global Change Postdoctoral Fellowship Program, and NSF grant AGS-1417659. This collaborative research emerged from Tra Dinh's visit to the Laboratoire de Météorologie Dynamique, which was supported by the "Tropical Cirrus" project of École Polytechnique's "Chaire pour le Développement Durable." Aurélien Podglajen, Albert Hertzog, Bernard Legras and Riwal Plougonven received support from the ANR project "Stradyvarius" (ANR-13-BS06-0011-01).

References

Barahona, D. and Nenes, A.: Parameterization of cirrus cloud formation in large-scale models: homogeneous nucleation, J. Geophys. Res., 113, D11211, doi:10.1029/2007JD009355, 2008. 8773

Boccara, G., Hertzog, A., Vincent, R. A., and Vial, F.: Estimation of gravity-wave momentum fluxes and phase speeds from quasi-Lagrangian stratospheric balloon flights. Part I: Theory and simulations, J. Atmos. Sci., 65, 3042–3055, doi:10.1175/2008JAS2709.1, 2008. 8774, 8775

Brewer, A. W.: Evidence for a world circulation provided by the measurements of helium and water vapour distribution in the stratosphere, Q. J. Roy. Meteor. Soc., 75, 351–363, doi:10.1002/qj.49707532603, 1949. 8772

Chen, Y., Kreidenweis, S. M., McInnes, L. M., Rogers, D. C., and DeMott, P. J.: Single particle analyses of ice nucleating aerosols in the upper troposphere and lower stratosphere, Geophys. Res. Lett., 25, 1391–1394, doi:10.1029/97GL03261, 1998. 8773, 8776

Corti, T., Luo, B. P., Fu, Q., Vömel, H., and Peter, T.: The impact of cirrus clouds on tropical troposphere-to-stratosphere transport, Atmos. Chem. Phys., 6, 2539–2547, doi:10.5194/acp-6-2539-2006, 2006. 8772

Davis, S., Hlavka, D., Jensen, E., Rosenlof, K., Yang, Q., Schmidt, S., Borrmann, S., Frey, W., Lawson, P., Voemel, H., and Bui, T. P.: In situ and lidar observations of tropopause subvisible cirrus clouds during TC4, J. Geophys. Res., 115, D00J17, doi:10.1029/2009JD013093, 2010. 8773

Dinh, T. and Durran, D. R.: A hybrid bin scheme to solve the condensation/evaporation equation using a cubic distribution function, Atmos. Chem. Phys., 12, 1003–1011, doi:10.5194/acp-12-1003-2012, 2012. 8776

Dinh, T. and Fueglistaler, S.: Cirrus, transport, and mixing in the tropical upper troposphere, J. Atmos. Sci., 71, 1339–1352, doi:10.1175/JAS-D-13-0147.1, 2014a. 8772

Dinh, T. and Fueglistaler, S.: Microphysical, radiative and dynamical impacts of thin cirrus clouds on humidity in the tropical tropopause layer and stratosphere, Geophys. Res. Lett., 41, 6949–6955, doi:10.1002/2014GL061289, 2014b. 8772

Dinh, T., Durran, D. R., and Ackerman, T.: Cirrus and water vapor transport in the tropical tropopause layer – Part 1: A specific case modeling study, Atmos. Chem. Phys., 12, 9799–9815, doi:10.5194/acp-12-9799-2012, 2012. 8787

Dinh, T., Fueglistaler, S., Durran, D., and Ackerman, T.: Cirrus and water vapour transport in the tropical tropopause layer – Part 2: Roles of ice nucleation and sedimentation, cloud dynamics, and moisture conditions, Atmos. Chem. Phys., 14, 12225–12236, doi:10.5194/acp-14-12225-2014, 2014. 8787

Fueglistaler, S., Dessler, A. E., Dunkerton, T. J., Folkins, I., Fu, Q., and Mote, P. W.: Tropical tropopause layer, Rev. Geophys., 47, RG1004, doi:10.1029/2008RG000267, 2009. 8772

Jensen, E. J., Toon, O. B., Pfister, L., and Selkirk, H. B.: Dehydration of the upper troposphere and lower stratosphere by subvisible cirrus clouds near the tropical tropopause, Geophys. Res. Lett., 23, 825–828, doi:10.1029/96GL00722, 1996. 8772

ACPD
15, 8771–8799, 2015

Jensen, E. J., Pfister, L., Bui, T.-P., Lawson, P., and Baumgardner, D.: Ice nucleation and cloud microphysical properties in tropical tropopause layer cirrus, Atmos. Chem. Phys., 10, 1369–1384, doi:10.5194/acp-10-1369-2010, 2010. 8773

Jensen, E. J., Pfister, L., and Bui, T. P.: Physical processes controlling ice concentrations in cold cirrus near the tropical tropopause, J. Geophys. Res., 117, D11205, doi:10.1029/2011JD017319, 2012. 8773

Jensen, E. J., Diskin, G., Lawson, R. P., Lance, S., Bui, T. P., Hlavka, D., McGill, M., Pfister, L., Toon, O. B., and Gao, R.: Ice nucleation and dehydration in the Tropical Tropopause Layer, P. Natl. Acad. Sci. USA, 110, 2041–2046, doi:10.1073/pnas.1217104110, 2013. 8787, 8788

Kärcher, B. and Lohmann, U.: A parameterization of cirrus cloud formation: Homogeneous freezing of supercooled aerosols, J. Geophys. Res., 107, AAC4.1–AAC4.10, doi:10.1029/2001JD000470, 2002. 8777

Kärcher, B., Dörnbrack, A., and Sölch, I.: Supersaturation variability and cirrus ice crystal size distributions, J. Atmos. Sci., 71, 2905–2926, doi:10.1175/JAS-D-13-0404.1, 2014. 8772

Koop, T., Luo, B., Tsias, A., and Peter, T.: Water activity as the determinant for homogeneous ice nucleation in aqueous solutions, Nature, 406, 611–614, doi:10.1038/35020537, 2000. 8776, 8777, 8782, 8783

Krämer, M., Schiller, C., Afchine, A., Bauer, R., Gensch, I., Mangold, A., Schlicht, S., Spelten, N., Sitnikov, N., Borrmann, S., de Reus, M., and Spichtinger, P.: Ice supersaturations and cirrus cloud crystal numbers, Atmos. Chem. Phys., 9, 3505–3522, doi:10.5194/acp-9-3505-2009, 2009. 8773, 8778

Lawson, R. P., Pilson, B., Baker, B., Mo, Q., Jensen, E., Pfister, L., and Bui, P.: Aircraft measurements of microphysical properties of subvisible cirrus in the tropical tropopause layer, Atmos. Chem. Phys., 8, 1609–1620, doi:10.5194/acp-8-1609-2008, 2008. 8773

Lohmann, U. and Roeckner, E.: Influence of cirrus cloud radiative forcing on climate and climate sensitivity in a general circulation model, J. Geophys. Res., 100, 16305, doi:10.1029/95JD01383, 1995. 8772

Magee, N., Moyle, A. M., and Lamb, D.: Experimental determination of the deposition coefficient of small cirrus-like ice crystals near −50° Celsius, Geophys. Res. Lett., 33, L17813, doi:10.1029/2006GL026665, 2006. 8776

Massman, W. J.: On the nature of vertical oscillations of constant volume balloons, J. Appl. Meteorol., 17, 1351–1356, doi:10.1175/1520-0450(1978)017<1351:OTNOVO>2.0.CO;2, 1978. 8774

ACPD
15, 8771–8799, 2015

Nastrom, G. D.: The response of superpressure balloons to gravity waves, J. Appl. Meteorol., 19, 1013–1019, doi:10.1175/1520-0450(1980)019<1013:TROSBT>2.0.CO;2, 1980. 8774
Podglajen, A., Hertzog, A., Plougonven, R., and Žagar, N.: Assessment of the accuracy of (re)analyses in the equatorial lower stratosphere, J. Geophys. Res., 119, 11166–11188, doi:10.1002/2014JD021849, 2014. 8774
Pruppacher, H. R. and Klett, J. D.: Microphysics of clouds and precipitation, D. Reidel Publishing Company, Dordrecht, Holland, 1978. 8776
Rabier, F., Bouchard, A., Brun, E., Doerenbecher, A., Guedj, S., Guidard, V., Karbou, F., Peuch, V.-H., Amraoui, L. E., Puech, D., Genthon, C., Picard, G., Town, M., Hertzog, A., Vial, F., Cocquerez, P., Cohn, S. A., Hock, T., Fox, J., Cole, H., Parsons, D., Powers, J., Romberg, K., VanAndel, J., Deshler, T., Mercer, J., Haase, J. S., Avallone, L., Kalnajs, L., and Mechoso, C. R.: The Concordiasi project in Antarctica, B. Am. Meteorol. Soc., 91, 69–86, doi:10.1175/2009bams2764.1, 2010. 8774
Ren, C. and Mackenzie, A. R.: Cirrus parametrization and the role of ice nuclei, Q. J. Roy. Meteor. Soc., 131, 1585–1605, doi:10.1256/qj.04.126, 2005. 8777
Rogers, D. C., Demott, P. J., Kreidenweis, S. M., and Chen, Y.: Measurements of ice nucleating aerosols during SUCCESS, Geophys. Res. Lett., 25, 1383–1386, doi:10.1029/97GL03478, 1998. 8773
Skrotzki, J., Connolly, P., Schnaiter, M., Saathoff, H., Möhler, O., Wagner, R., Niemand, M., Ebert, V., and Leisner, T.: The accommodation coefficient of water molecules on ice – cirrus cloud studies at the AIDA simulation chamber, Atmos. Chem. Phys., 13, 4451–4466, doi:10.5194/acp-13-4451-2013, 2013. 8776
Spichtinger, P. and Krämer, M.: Tropical tropopause ice clouds: a dynamic approach to the mystery of low crystal numbers, Atmos. Chem. Phys., 13, 9801–9818, doi:10.5194/acp-13-9801-2013, 2013. 8773, 8779, 8787
Vincent, R. A. and Hertzog, A.: The response of superpressure balloons to gravity wave motions, Atmos. Meas. Tech., 7, 1043–1055, doi:10.5194/amt-7-1043-2014, 2014. 8774

ACPD
15, 8771–8799, 2015

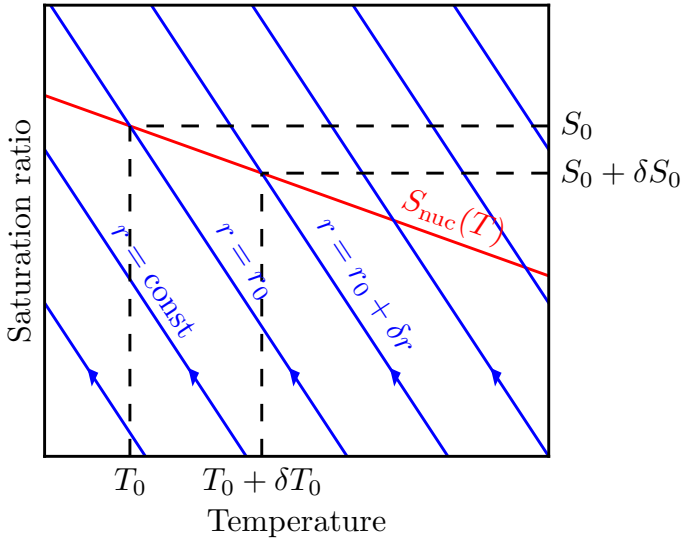

Figure 1. Diagram illustrating the initial conditions of the air parcels. Prior to nucleation air parcels follow isolines of water vapour mixing ratio r (shown here in blue) and approach the curve $S_{\mathrm{nuc}}(T)$ from below (as indicated by the arrows). Nucleation begins at the intersections of the r isolines with the curve $S_{\mathrm{nuc}}(T)$.

ACPD
15, 8771–8799, 2015

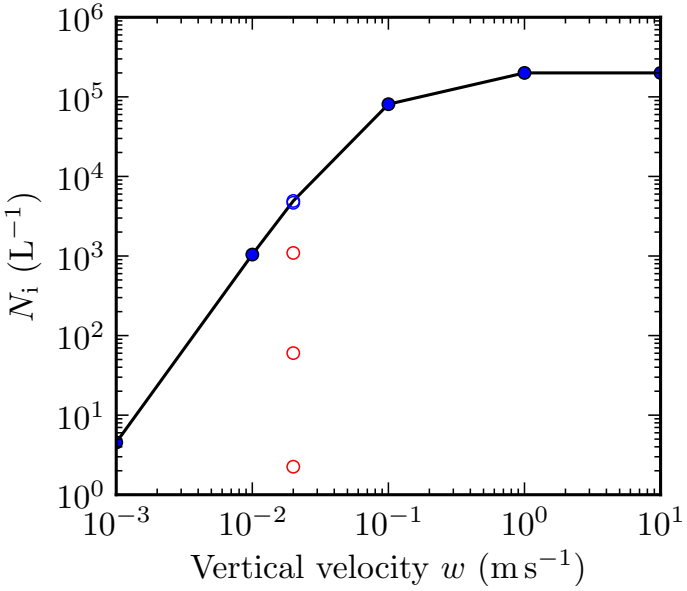

Figure 2. Number of ice crystals obtained for the five nucleation events forced by constant $w = \{0.001; 0.01; 0.1; 1; 10\}\,m\,s^{-1}$ (solid circles), and the five nucleation events forced by $w = \pm 0.02\,m\,s^{-1}$, see Eq. (7) (open circles). Vapour-limit events (blue circles) are obtained with constant w, or with $w = \pm 0.02\,m\,s^{-1}$ and $t_s = \{32; 36\}$ min. Temperature-limit events (red circles) are obtained with $w = \pm 0.02\,m\,s^{-1}$ and $t_s = \{20; 24; 28\}$ min. The INCs are almost the same for the two vapour-limit events obtained with $w = \pm 0.02\,m\,s^{-1}$, hence the two open blue circles overlap.

ACPD
15, 8771–8799, 2015

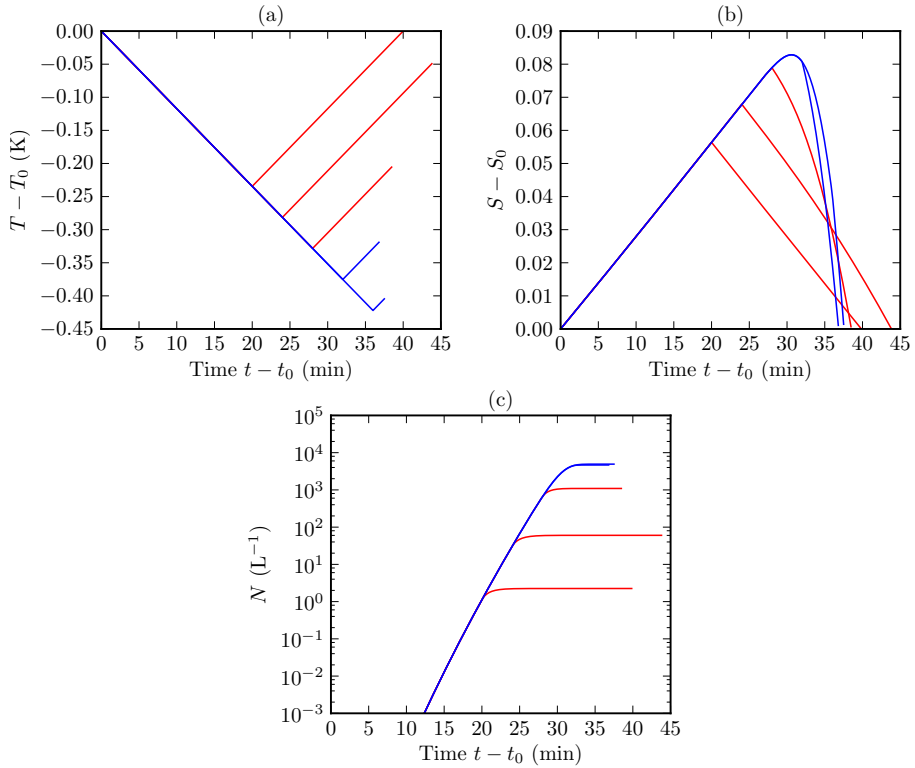

Figure 3. Evolution of temperature, saturation ratio and INC during the five nucleation events forced by $w = \pm 0.02\,\mathrm{m\,s^{-1}}$ as defined by Eq. (7). Blue curves show vapour-limit events and red curves show temperature-limit events.

ACPD
15, 8771–8799, 2015

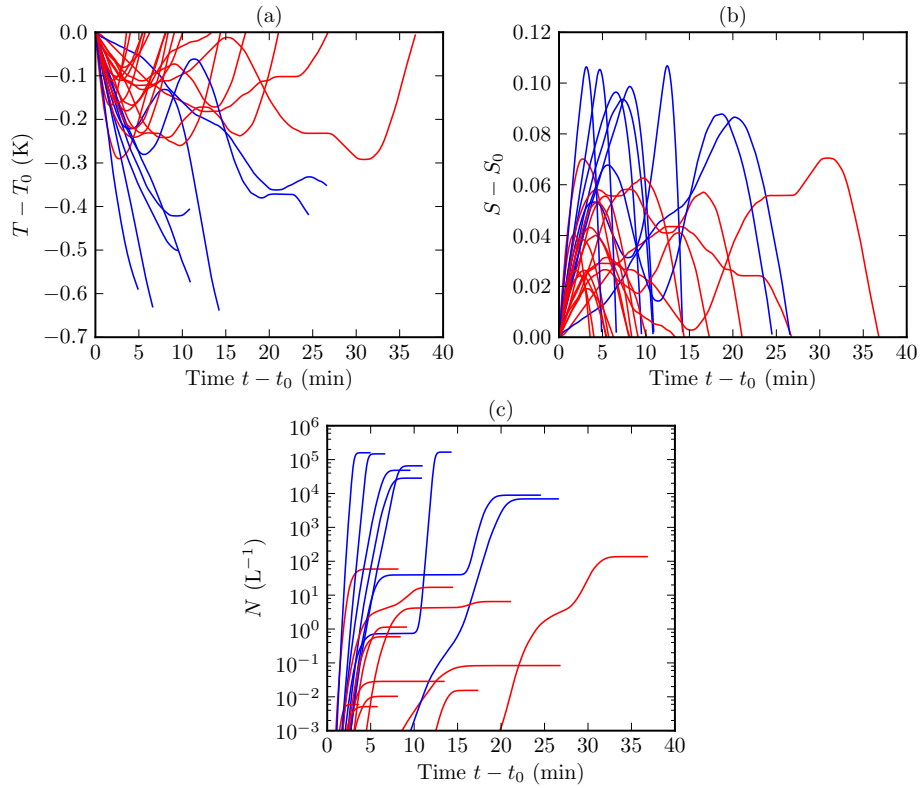

Figure 4. Same as Fig. 3 but for nucleation events forced by the temperature perturbations taken from the balloon data.

ACPD
15, 8771–8799, 2015

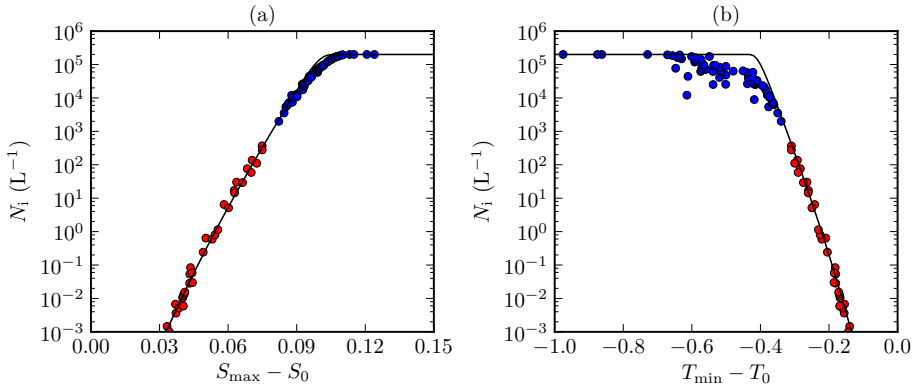

Figure 5. Number of ice crystals nucleated at $T_0 = 195\,K$ with the balloon temperature perturbation time series. Blue circles show vapour-limit nucleation events. Red circles show temperature-limit nucleation events. The solid curve is obtained from Eqs. (16)–(20) with $\mu = 0.02\,s^{-1}$.

ACPD
15, 8771–8799, 2015

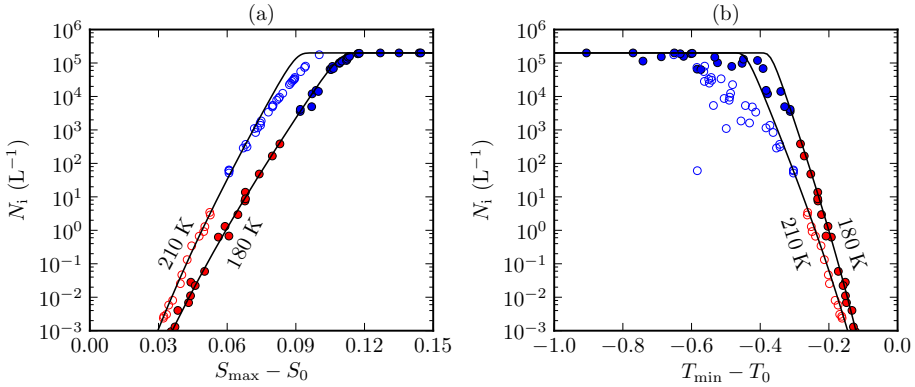

Figure 6. Same as Fig. 5 but for T_0 = 180 K (solid circles) and 210 K (empty circles).

ACPD
15, 8771–8799, 2015

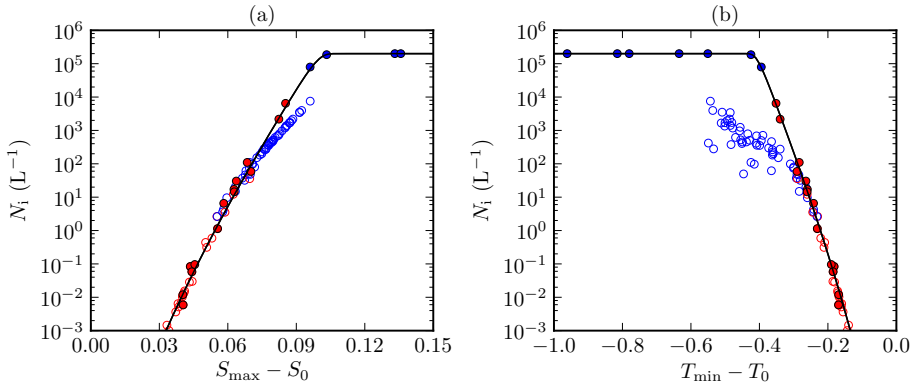

Figure 7. Same as Fig. 5 but for α = 0.001 (solid circles) and α = 1 (empty circles).

ACPD
15, 8771–8799, 2015

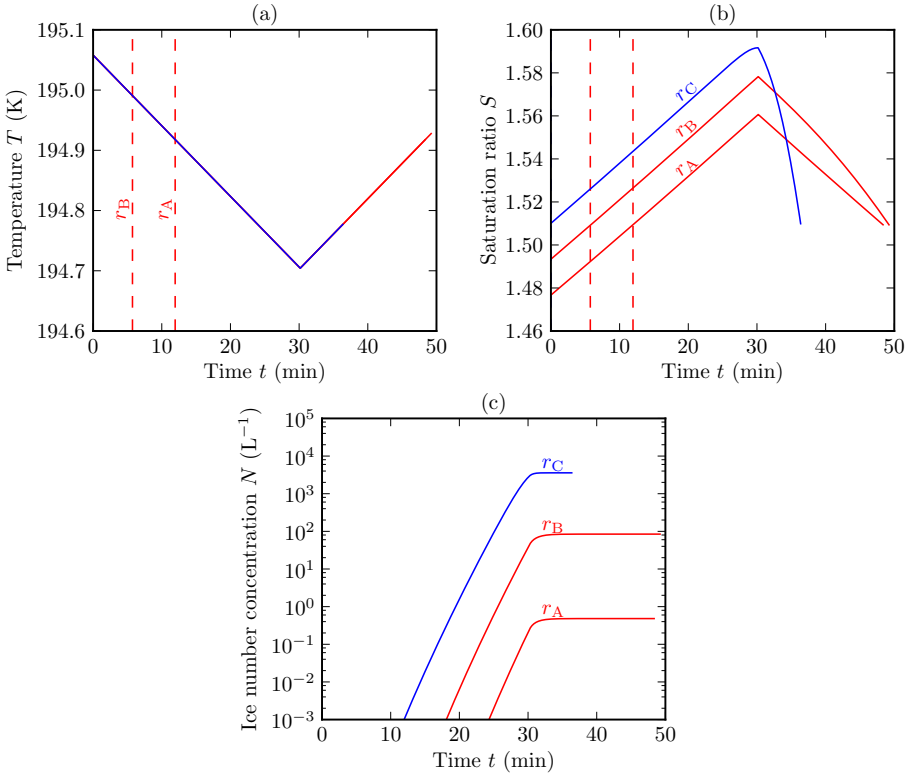

Figure 8. Evolution of temperature, saturation ratio and INC for three air parcels with slightly different initial water vapour mixing ratios: $\{r_A = 1.77;\ r_B = 1.79;\ r_C = 1.81\} \times 10^{-5}$ kg kg^{-1}. The three parcels follow the same temperature time series as shown in **(a)**, but the differences in their initial water vapour contents result in widely different INCs. The two dry parcels experience temperature-limit (red) events, which begin at the times indicated by the dash lines in **(a)** and **(b)**. The moist parcel experiences a vapour-limit (blue) event, which starts from $t = 0$.

ACPD
15, 8771–8799, 2015